Letters in Applied NanoBioScience
Open-Access Journal (ISSN: 2284-6808)

Article
Volume 12, Issue 2, 2023, 60
https://doi.org/10.33263/LIANBS122.060

Investigation of Thermal and Structure Properties of Silk Dyed with a Natural Dye

Rabab I. Mahmoud [1,*], Nabawia A. Adelzaher [2]

[1] Textile Meteology Lab., Chemical Metrology Devision 1, India
[2] Textile Meteology Lab., Chemical Metrology Devision 2, India
* Correspondence: rabab200@yahoo.com;

Scopus Author ID 7004637202
Received: 7.09.2021; Accepted: 20.02.2022; Published: 23.03.2022

Abstract: The present work aimed to dye silk fabric with natural dye extracted from the Artemisia Herba Alba plant from its leaves on pure silk dyeing fabrics with different dyeing conditions such as time, temperature, and pH value in the presence of Alum as a mordant, which had given different colors and shades to promote the use of natural silk fiber. Optimum results were obtained. Silk fabric was dyed using pH 5 for 45 minutes at temperature 80^{o}C and 1:40 liquor ratio. Finally, the dyed mordant samples were thoroughly washed and dried at ambient conditions. The results obtained us successfully characterized dyed silk fabric by studying with a Fourier Transform Infrared thermogravimetric (TGA) properties, (FTIR) analysis technique, and X-ray diffraction (XRD). Improvement in the dyeing process may have been attributed to the improvement in the molecular structure of the chemical bonds in silk fabrics. This work gives an opportunity to use a new traditional natural dye that meets the future environmental technology that exhibited fantastic dyed patterns of high quality.

Keywords: Artemisia Herba Alba plant; silk fabric; optical properties; XRD; FTIR and thermal properties.

1. Introduction

Artemisia herba-alba (or white wormwood) had a specific epithet herba-alba means "white herb" in Latin, as its stems and leaves were white and woolly [1]. Similarly, it has armoise herbe-blanche or armoise blanche in French. In Arabic, it is shīeh [2]. And it is la'anah in Old Testament Hebrew [3,4]. It is a perennial shrub in the genus Artemisia that grows commonly on the dry steppes of the Mediterranean regions in Northern Africa (Saharan Maghreb), Western Asia (Arabian Peninsula), and Southwestern Europe [5]. It is used as an antiseptic and antispasmodic in herbal medicine. Its structure depends on the place to be extracted, it primarily contains 1,8-cineole and appreciable amounts of alpha and beta-thujone as well as other oxygenated monoterpenes, including terpinen-4-ol, camphor, and borneol [6] from (Sinai Desert), while the other extracted from (Morocco [7] and Spain [8]) includes proghanone, chrysanthenone, and cis-chrysanthenol. These constituents were listed as major constituents. Another source contains less common non-head-to-tail monoterpene (i.e., santolin and yomogi alcohol [9]) alcohols. Also, sources collected from (aerial parts in Egypt [10]) containing Eudesmanolide and germacranolide sesquiterpenes were detected in methanol and two bioactive flavonoids in ethyl acetate, supposed to be hispidulin and cirsiliol [11]. Silk, a well-known natural fiber produced by the silkworm Bombyx mori L, consists of fibroin and

glue-like sericin. One-third of the fibroin exhibits an amorphous region, and two-thirds of the fibroin demonstrates a crystalline component. The crystalline component consists of two forms, silk I and silk II. Silk II, the fiber structure after spinning, mainly consists of an anti-parallel β-sheet that is thermodynamically the most stable [12,13]. Silk I, the conformation of fibroin in the solid-state before spinning, is unstable. Many factors can structurally convert silk I into silk II, such as shearing, hydration, heat treatment [14-17], polar solvents, and macromolecules that contain carbonyl or polar groups [18,19]. Recently, silk fibroin has been gradually perceived for its biocompatibility, biodegradability, excellent mechanical properties, and optical performance. Thus, the development and application of silk fibroin in biomedical materials have gained increasing attention [20].

The silk fiber is 75% fibroin and 25% sericin. The silk fiber is composed of 18 amino acids with various reactive functional groups, including hydroxyl and amine groups [21] (natural protein or polypeptide). Natural polyamino acid biopolymers in arthropod-forming organisms (as polypeptides [22] or proteins) are synthesized from amino acid (– NH – CHR – CO –) and imino acid (– NR1–CHR2–CO –) monomas. The H – L complex [23,24] also binds glycoprotein P25 in a ratio of 6:1 via hydrophobic interactions to form an elementary micellar unit by forming a large amount of fibroin to be transported through the lumen of the silk gland towards the spinnerets before spinning [25,26] into fibers,). The presence of sericins streng in the silk fiber lacks luster; thus, we must be degummed before dying [27]. Previously studied stated that residual sericin improves the wet spin capacity, post drawing, and mechanical properties of silk [28,29]. (Also previously mentioned is the fact that residual sericin can boost electro-spinability [30] and its rate [31] for regenerated silk.

In this article, we successfully characterized dyed silk fabric (SF) with natural dye by studying with a Fourier Transform Infrared (FTIR) analysis technique, X-ray diffraction (XRD), and thermogravimetric (TGA) properties

2. Materials and Methods

2.1. Chemicals & materials.

A commercially scoured and bleached silk fabric (55g/m^2 in weight and 0.06 cm in thickness) produced in Akhmeem, Egypt, were used for investigation without any purification., and Aluminum Potassium Sulfate (Al $K(SO_4)_2 \cdot 12H_2O$), which was used as a mordant in a pure state. With the use of a natural dye named Artemisia Herba Alba.

2.2. Dye extraction procedure.

Dried leaves of Artemisia Herba-Blanche (with Arabic name EL-Shieh) were used for obtaining natural dye then crushed. Take 50 gm of this natural dye crushed in 500 ml of distilled water and allowed to boil for one hour, then filtrated that solution to drain the undesired portions to obtain a clear solution for use in the dyeing process [32].

2.3. Dyeing process.

Silk fabrics were dyed with the Artemisia Herba Alba extract dye solution with a liquor ratio of 1:50 based on the weight (50 % owf.). All fabrics were pre-mordant with 6 g / Liter concentration of Alum (Potassium and Aluminum Sulfate) before dyeing. Then, dyed silk fabrics were divided into three groups. The first group was dyed in dye baths of different pH

values (2,3,4,5,6 and 9) at a temperature of 60°C for 45 minutes. The second group was dyed at pH = 5, 60oC temperature for 15,30, 45, 60, and 90 minutes for different periods. For different temperatures of 40, 60, 80, and 100°C, the third group was dyed for 45 minutes and pH = 5 in a dyed bath. The samples under test were dyed separately by the pre-extracted dye in a laboratory dyeing apparatus using the conventional exhaustion dyeing method [33].

2.4. Thermal analysis.

Thermal behavior of the silk dyed with Artemisia was measured by Thermogravimetric Analyzer model Shimadzu TGA-60H (Kyoto, Japan) from 20 to 200°C. A heating rate of 10 °C/minute was used under a dry nitrogen atmosphere and 20 ml/minute flow rate. The dry sample weight was about 2.41 mg. samples runs were repeated at least three times to ensure the reproducibility scans were started at 10°C and ran to a final temperature of 650°C. The instrument was calibrated using calcium oxalate, which was supplied along with the instrument; the uncertainty value of the sample mass measurement is ± 1%.

2.5. Fourier Transform Infrared (FTIR) spectroscopy.

The FTIR spectrum of both colored and undyed silk fabric is recorded using Nicolet 380 spectrophotometer with Attenuation Total Reflection (ATR) mode with zinc selenide crystal, 4000-650 cm^{-1} spectral range, to ensure reproducible contact between the crystal face and the fabric pressure of approximately 18Kpa was applied to the crystal holder, 4 cm-1 resolution and 32 scans. Minute samples were collected from brittle paint layer areas using a syringe needle (0.3 mm diameter) and measured on diamond cells (Spectra tech. Shelton,(Ct. USA).

2.6. X-ray (XRD) diffraction spectrometer.

The sample patterns of X-ray diffraction spectrometers were analyzed in a continuous mode X-ray diffraction instrument (PAN-analytical X'Pert PRO) using a Cu target, Ni-filtered Cu-Kα radiation (λ = 1.540598 Å) was used as an X-ray source at 30 KV and 20 mA. All scans were performed at a speed rate of 2 degrees/minute, with a step size of 0.6. With a step size of 2θ = 0.013, ranging from 2θ =5-80o ranges. The morphology characterization was made in the Netherlands model Field Emission, Emperyaen. The crystallinity index (CI) was calculated using empirical Degal's relation [34-36].

$$D = \frac{K\,\lambda}{\beta\ cos\theta}$$ Crystallite size (D) by Debye-Sherrer formula

K: shape factor (0.89-1.39), β: FWHM of the observed peak (rad), λ: wavelength of the x-ray (1.5406 A°, and θ: angle of incidence (rad).

$$C.I.(\%) = \frac{hc}{ht}x\ 100$$ Crystallinity Index (C.I.) by Degal's relation

hc: height of main crystalline peak and ht: total height of the main crystalline peak

3. Results and Discussion

3.1. Characterization of extracted dye.

3.1.1. Ultraviolet-visible spectroscopy.

UV–visible transmittance measurements. The optical transmittances of the extracted dye were measured from 350 to 900 nm using a Shimadzu (VIS) Double Beam Spectrophotometer with standard illuminant C (1174.83) Model V-530 and bandwidth 2.0 nm cover the range 200-2500 nm with accuracy ± 0.05%. The evaluation of the optical density of the extract solution after filtration was measured by concentration.

Figure 1 indicates the absorption spectrum of the aqueous extract of the Artemisia Herba Alba leaves. It represents two peaks in the yellow color range: the first has λmax at 420 nm of optical density 2.77, and the second has λmax at 460 nm of optical density 1.55. The dried leaves of the Artemisia Herba Alba plant were found to discharge color in hot water very easily. Increasing the number of barks from 2 to 12 g per 1000 ml, water boiled for 1 hour is accompanied by the increase in color strength and depth in color. The maximum absorbance of extract solution has at wavelength λmax =330 nm in the UV absorbance range.

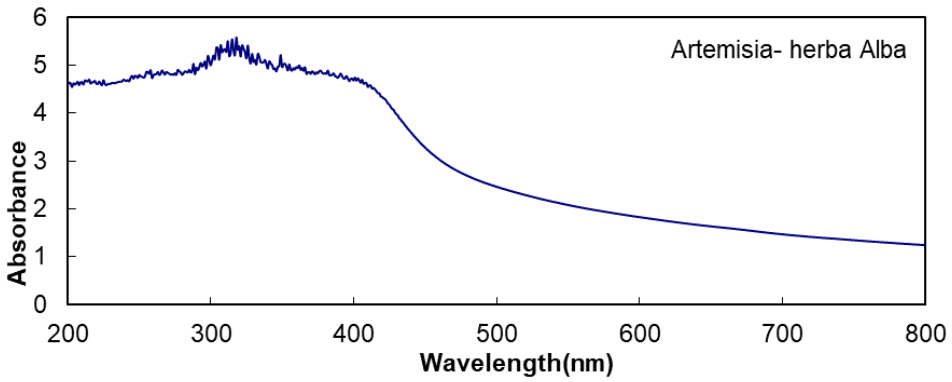

Figure 1. The absorbance spectrum of extract of Artemisia Herba Alba leaves all over the UV-Vis range.

3.2. Characterization of Silk Dyed with Artemisia herba-alba leaves.

3.2.1. Thermal analysis.

TGA is commonly used to investigate the thermal decomposition of polymers to determine kinetic parameters like activation energy and reaction order; these parameters can be used to gain a better understanding of the thermal stability of polymers, as well as to assess the importance of loss of fiber moisture in addition to traditional methods [37].

During this analysis, three conditions (pH value, time, and temperature) were used to achieve the best condition for dyeing with natural dye (*Artemisia herba-alba*) and then to test thermally for all three groups to detect the optimal conditions.

In the first step, the weight loss corresponding to the evaporation of bound water (desorption of water physically bound to fiber and dehydration of silk) produces a broad/sharp endothermal peak and ends at approximately 90-100^{o}C. Therefore the initial weight arising from the departure of moisture appeared from room temperature up to around 100^{o}C. The melting temperature of silk fabric is well known to decrease with rising moisture content. The second loss peak beginning above 200^{o}C is due to crystal cleavage (as seen in figure 2). It can be due to the melting and dehydration of various morphological components that make up the

extremely complicated silk structure—a weight loss caused by protein fiber structure decomposition.

Some work on the thermal behavior of silk proteins in silkworms [38], if silk fibroins in the form of α, β lose water on heating up to 100° C and molecular movement start at 175° C in the crystalline regions, and transition at 270° C, the other type of silk sericin undergoes a glass transformation at 170° C. It crystallizes at 250° C. Glass transition temperatures of wild silk fibroins differ with species of silkworms ranging from 160 to 210°C. As amorphous random-coil fibroin increased temperature, the water evaporated to 100 ° C, Intra- and intermolecular hydrogen bonds between 150 and 180° C are broken. The vertical transition is observed at 175° C. The transformation from random-coil to β-shaped, followed by hydrogen bond reformation above 180° C and crystallization above 190° C.

Table 1. The Weight loss of undyed and dyed silk using natural dye (*Artemisia herba-alba*) with different pH values at 45min. Temperature 80ºC and L:R. 1:40.

pH	First step		Second step		Third step		Total step	
	weight loss %	Mid-point (ºC)	weight loss %	Mid-point (ºC)	weight loss %	Mid-point (ºC)	weight loss %	Mid-point (ºC)
Blank	-24.374	240.05	-38.442	304.58	-14.133	386.45	-71.028	312.52
2	-17.400	284.06	-26.060	317.79	-11.332	380.01	-70.170	310.86
3	-24.476	294.88	-27.384	322.93	-19.735	408.07	-73.608	315.66
4	-28.004	308.75	-31.207	329.78	-20.036	441.01	-74.628	318.61
5	-33.790	376.16	-44.045	387.59	-23.713	491.84	-76.609	328.30
6	-31.538	332.21	-38.511	343.88	-17.937	439.73	-69.690	310.98
9	-21.205	286.06	-26.106	300.37	-15.794	323.32	-67.400	307.44

By observing Figure 2 and Table 1 representing the First group (I) a change in the pH of the dye solution, it is noted that the first step of weight loss and the Midpoint temperature corresponding to the evaporation of water physically bound to fiber as a result of silk dehydration as seen in the first step of weight loss increases for all samples in this group that are dyed from pH 2 to 5 then decrease from 6 to 9 pH value. In the second step of weight loss (decomposition state), the weight loss occurs for the undyed silk sample (38.442%) of char residues. The weight loss increased from 2 to 5 pH value then decreased again from 6 to 9 with the lowest value (26.106%) of char residues this means that the best percentage of silk dyed with pH 5.

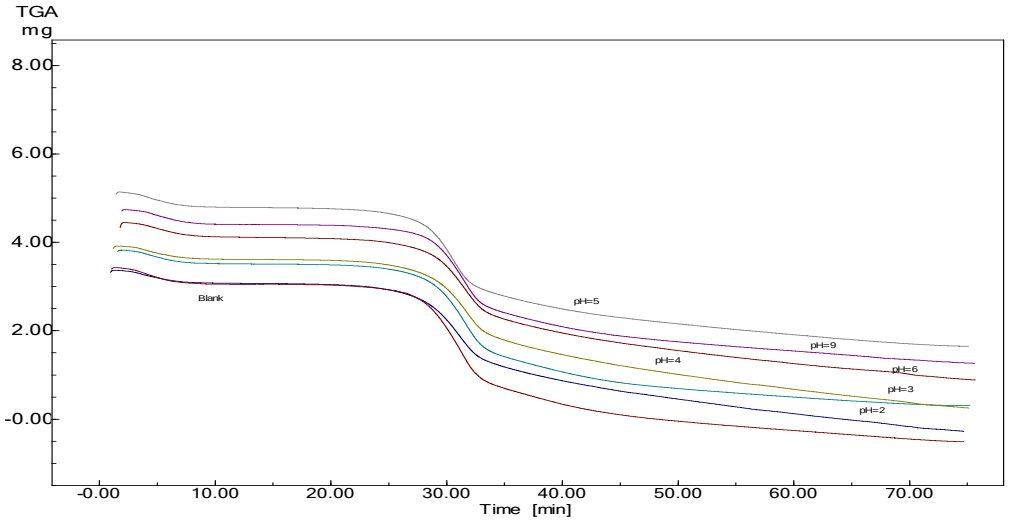

Figure 2. Typical TGA thermograms of undyed and dyed silk by *Artemisia herba-alba* with variation pH value at time 45min.and temperature 80oC and L:R. 1:40.

The third stage of decomposition showed that the lowest value of the weight loss in this stage is that for undyed silk sample (14.133%) and the value of weight loss also increased up to pH 5 then decreased again, it is clear that the difference between the weight loss at this stage compared to the undyed silk is due to pH value used.

As appearing in Figure 3 and Table 2 representing the second group (II) a time/min shift in the dye cycle, time period shows a distinct weight loss in three phases the first weight loss occurs more than 240.0 ° C, primarily due to the diffusion and decomposition step as seen in the first step of weight loss increases for all samples in this group that are dyed from 15 to 45 min. then decrease from 60 to 90 min. At the same time, the second stage with a weight loss of (44.476 %) due to the decomposition of silk fabrics begins at around more than 300.0 ° C. The second step of weight loss increased from 15 to 45 min. then decreased again by increasing time with the lowest value (28.077%) of char residues. This means that the best percentage of silk dyed with 45 min.

Table 2. The weight loss of undyed and dyed silk using natural dye (*Artemisia herba-alba*) at different times, at pH 5, temperature 80ºC and L:R 1:40.

time/ min.	First step		Second step		Third step		Total step	
	weight loss %	Mid-point (ºC)	weight loss %	Mid-point (ºC)	weight loss %	Mid-point (ºC)	weight loss %	Mid-point (ºC)
Blank	-24.374	240.05	-38.442	304.58	-14.133	386.45	-71.028	312.52
15	-16.386	281.20	-21.568	313.72	-21.862	438.06	-72.219	314.03
30	-24.840	293.25	-30.218	326.97	-24.488	455.82	-75.985	317.71
45	-34.088	364.64	-44.476	373.82	-28.077	474.22	-77.069	319.20
60	-30.653	286.24	-36.114	302.52	-20.733	455.01	-71.39	310.46
90	-22.344	257.63	-25.788	301.81	-15.535	451.32	-69.067	307.69

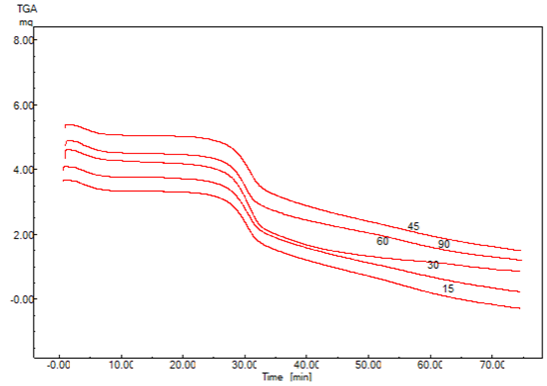

Figure 3. Typical TGA of undyed and dyed silk by *Artemisia herba-alba* with variation in time, with conditions pH 5, temperature 80ºC and L:R. 1:40

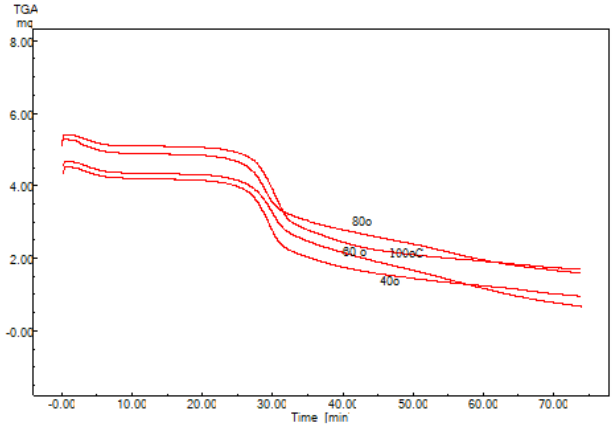

Figure 4. Typical TGA of undyed and dyed silk by *Artemisia herba-alba* with variation in temperature, with conditions pH 5 , time 45 min. and L:R. 1:40.

The third decomposition stage showed that the same progression with weight loss also increased to 45min. Then again decreased, it is obvious that the difference between the weight loss at this stage and the undyed silk implies that the Silk fabric wall can well protect n-octadecane. It is worthy of notice that n-octadecane exhibits a two-step thermal degradation cycle contrary to previous reports [39,40].

The third group (III) researched thermal analysis of changes in temperature during the dyeing process as shown in Table 3 and Fig. 4, showing a distinct weight loss in three phases. Weight loss percentage resulting in water evaporation physically attached to the fiber due to dehydration of the dyed silk fabric and weight loss increase for these samples which then decay from 40oC to 80^{o}C. And decrease with temperature increase up to 100^{o}C of the dyeing phase with the lowest weight loss value (2.907%), weight loss occurs between about 60°C and 70.44 °C, primarily due to the stage of diffusion and decomposition or the melting and dehydration of all components forming the highly complex structure of silk fiber [41]. For dyed silk fabric, the highest percentage was 80^{o}C. In the third decomposition stage, it was shown that at this point, the lowest weight loss value and the weight loss value increased to 80^{o}C and then decreased; it is clear that the difference between the weight loss at this point and the untouched silk is due to temperature variations during the dyeing process, the reduction in weight loss during dyeing is evident as a result of the presence of dye or mordant associated with such fabrics [39].

Table 3. The weight loss of the undyed and dyed silk by Artemisia Herba- Alba(as natural dye) with different temperatures, at pH 5 , time 45 min. and L:R 1:40.

Temperature (^{o}C)	First step		Second step		Third step		Total step	
	weight loss %	Mid-point (^{o}C)	weight loss %	Mid-point (^{o}C)	weight loss %	Mid-point (^{o}C)	weight loss %	Mid-point (^{o}C)
Blank	-24.374	240.05	-38.442	304.58	-14.133	386.45	-71.028	312.52
40^{o}C	-6.006	249.91	-31.742	297.63	-14.897	369.95	-68.577	304.1
60^{o}C	-10.617	269.16	-34.184	305.75	-21.805	395.38	-70.367	316.71
80^{o}C	-35.070	304.74	-44.331	339.31	-23.999	453.49	-76.388	316.34
100^{o}C	-26.622	290.84	-29.534	323.57	-21.27	494.16	-72.377	300.99

The value of the total weight loss at the end of the thermal degradation of the samples being tested indicates that the total weight loss of all samples dyed with natural dye in the presence of mordant (alum) with change in (pH, time, and temperature) have the lowest value, i.e., the char residue for this sample is the highest in weight [char residue = W1-W2]; where W1 is the total weight loss at the beginning of the thermal cycle, and W2 is the sample's total weight loss [42]. If the weight of the char residue is increased, it behaves as a carbonized replica of the original fabric and functions as a thermal barrier. The decomposition temperature of the fabrics is enhanced, the formation of flammable volatiles is decreased, and the fabrics show good flame retardancy when exposed to fire.

3.2.2. Fourier Transform Infrared (FTIR) spectroscopy.

3.2.2.1. FTIR of Artemisia herb alba (natural dye).

The FTIR Spectrum of extracted and purified dye is recorded using Perkin Elmer Spectrophotometer model 1650-USA with a wavenumber range of 4000-500 cm^{-1}. Figure 5 represents the FTIR spectra of Artemisia Herba Alba dye and the peak intensity value of characteristic functional bands. An important aspect in selecting a dye from a plant source is

the maximum color depth that can be obtained. Higher color depth is expected from an increase in extracted concentration. And the structural formula appears in Figure 6.

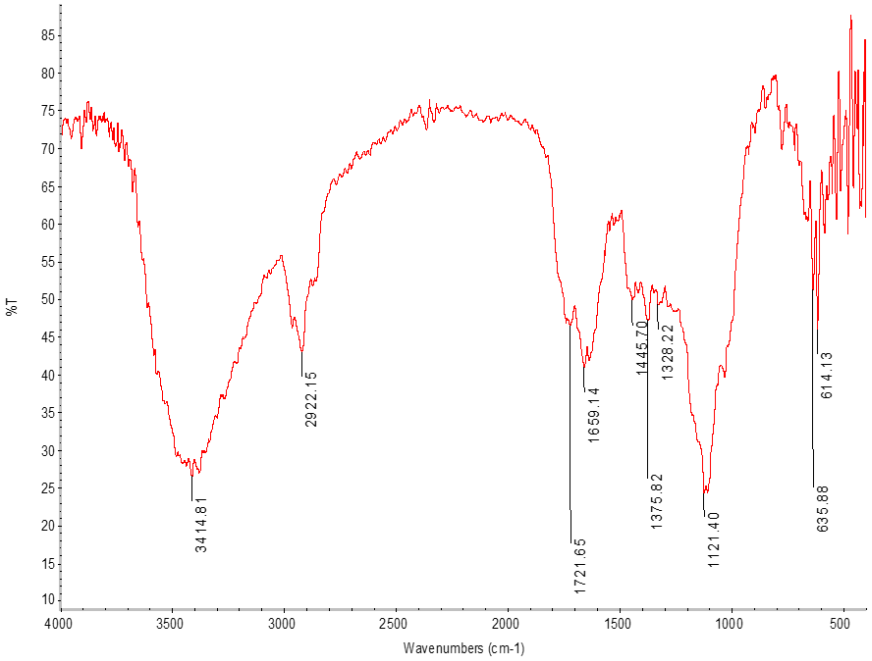

Figure 5. FTIR spectra of extracted Artemisia Herba Alba dye.

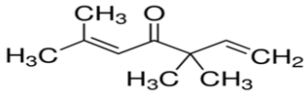

Figure 6. The structural formula of Artemisia herba Albadye.

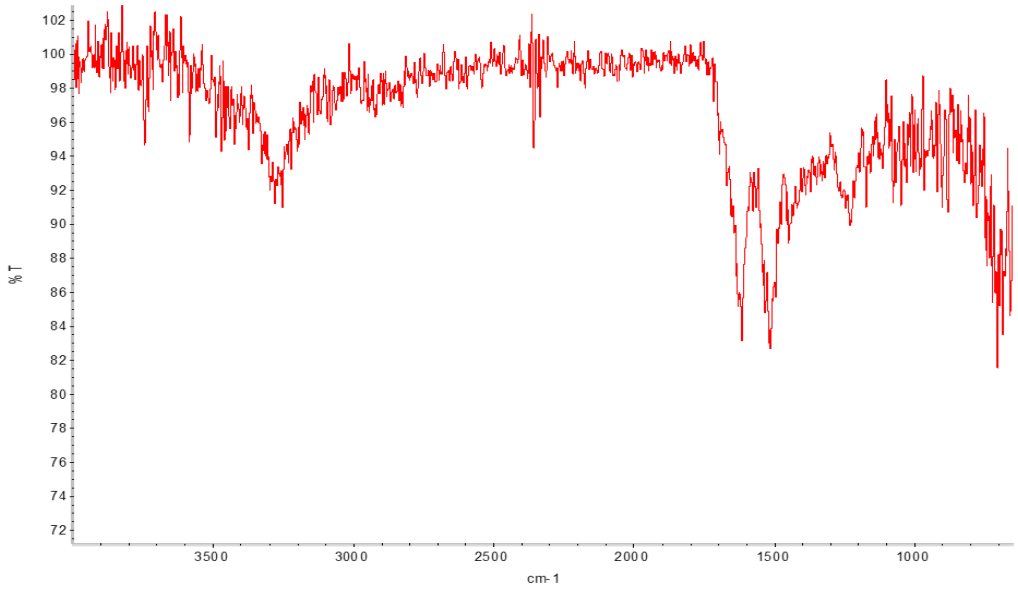

Figure 7. FTIR spectra of pure silk fabric.

The structural formula and FTIR of pure silk were observed in Figures 7, 8. The absorption bands at 1641 cm^{-1} and 1632 cm-1(amide I) and 1515 cm^{-1} (amide II) which is corresponding to (silk II) structure conformation as(β-sheet). Other absorption bands were observed at 1530 cm^{-1} (amide II), and 1237 cm^{-1} (amide III), which is characteristic of the (silk I) conformation of both random coil and α helix [43], the position at 1650 cm-1 (random coil) and 1630cm^{-1} (β-sheet) is associated to the C-O stretching of the amide I group [44,45], at 1540cm^{-1} (random coil), and 1520 cm^{-1}(β-sheet) corresponds to the N-H deformation of amide

II [46], at 1270 cm^{-1} (β-sheet), 1230 cm^{-1} (random coil) corresponding to the C-N stretching for amid III.

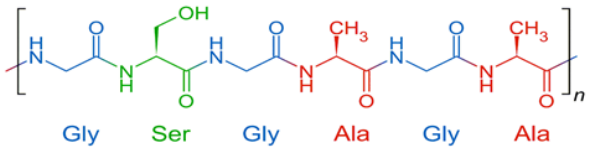

Figure 8. The structural formula of pure silk fabric.

Figure 9 indicate that the FTIR spectra of silk fabric dyed with *Artemisia herba-alba* (natural dye)at different pH value (first group I) and the characteristic IR bands of amide I and amide II were observed in the ranges of 1700–1550 cm^{-1} and 1550–1450 cm^{-1}. Because amino I and II are sensitive to secondary structures such α-helices and β- sheets, there were no significant conformational transformations during the self-assembly process. However, some slight differences in the bands of the CH_2 stretching vibration and amino III were observed. The weak absorption peaks of the CH_2 asymmetric and symmetric stretching vibration at 2924 and 2850 cm^{-1} were enhanced greatly, obviously silk macromolecules. Silk fibroin fiber consists of β-sheet crystals with heavy hydrogen bonding and a non-crystalline amorphous area with varying degrees of hydrogen bonding. The crystalline region of silk fibroin consists mainly of glycine residues which alternate with alanine and serine, whereas the amorphous region sequence contains a tyrosine-rich domain. The unconjugated tyrosine and amide residues in the protein backbone in the amorphous region can form intermolecular hydrogen-bonding interactions with hydrogen-donor or acceptor molecules, supplying other intermolecular attachment capabilities to the silk surface. This binding power is, however, greatly diminished.

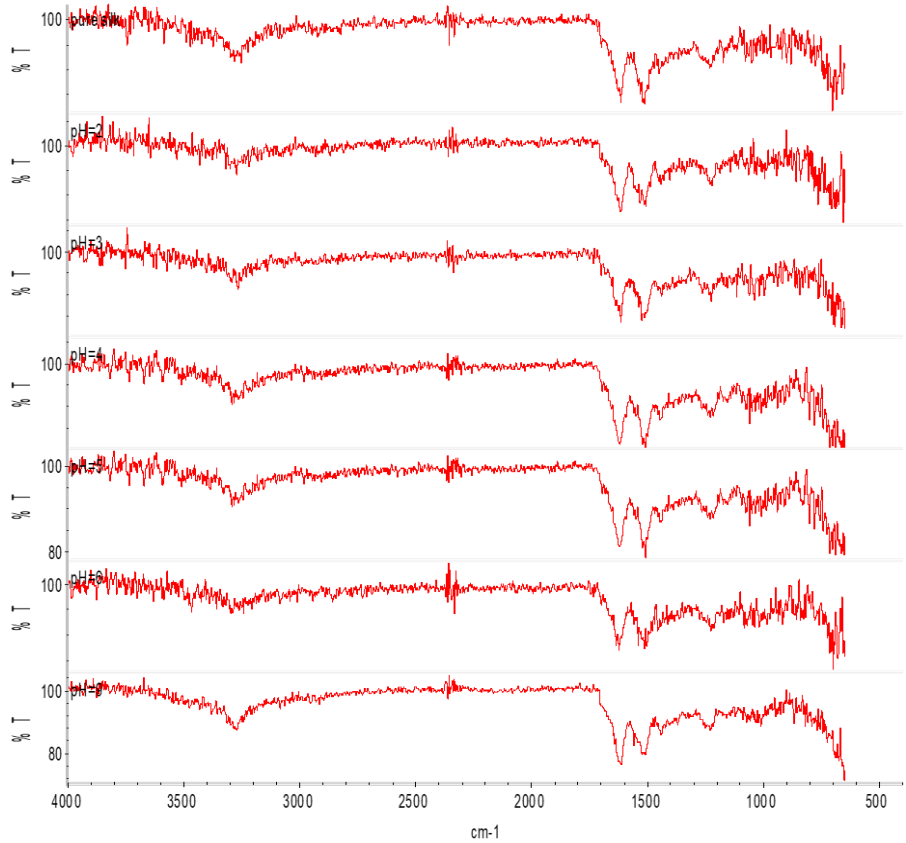

Figure 9. FTIR of dyed silk fabric with pH variation, condition time 45 min., temperature 80ºC and L:R. 1:40.

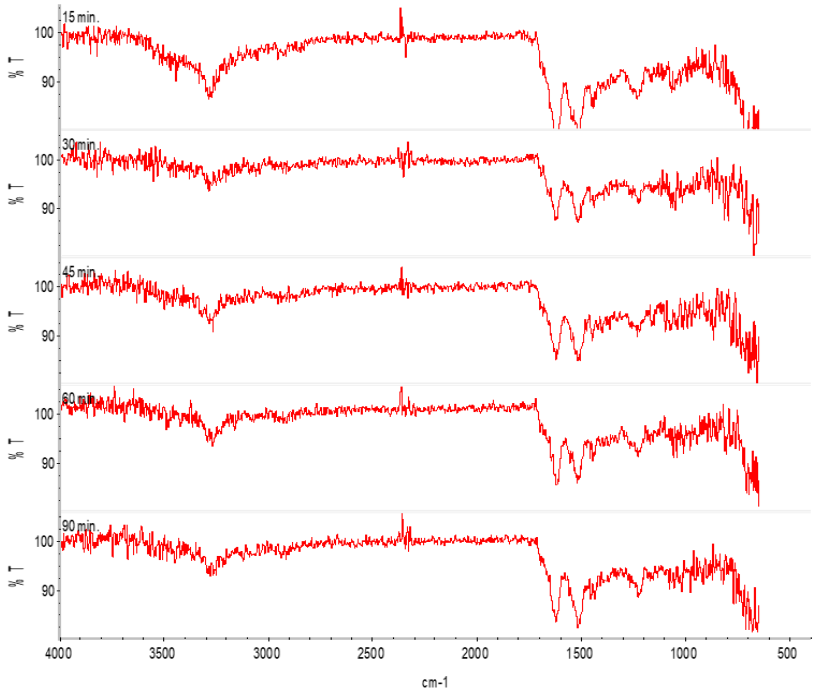

Figure 10. FTIR of dyed silk fabric with duration time, condition pH 5, temperature 80°C and L:R. 1:40.

The amide bands in FTIR spectra with duration time, which are known to be sensitive to silk fabric's molecular conformation. Figure 10 shows the FTIR spectra of all dyed silk fabric degummed for the different periods. All samples showed similar and strong bands at 1516 cm^{-1} (amide II), 1235 cm^{-1} (amide III), 965 cm-1 (amide IV), and 695 cm^{-1} (amide V), assigned to the β-sheet, and 1651 cm^{-1} (amide I) and 621 cm^{-1} (amide V), assigned to α-helix respectively. The similarity in FTIR spectra implies that the molecular conformation of degummed fibers did not change. They assume to both of β-sheet structure and random coil α-helix conformation [47].

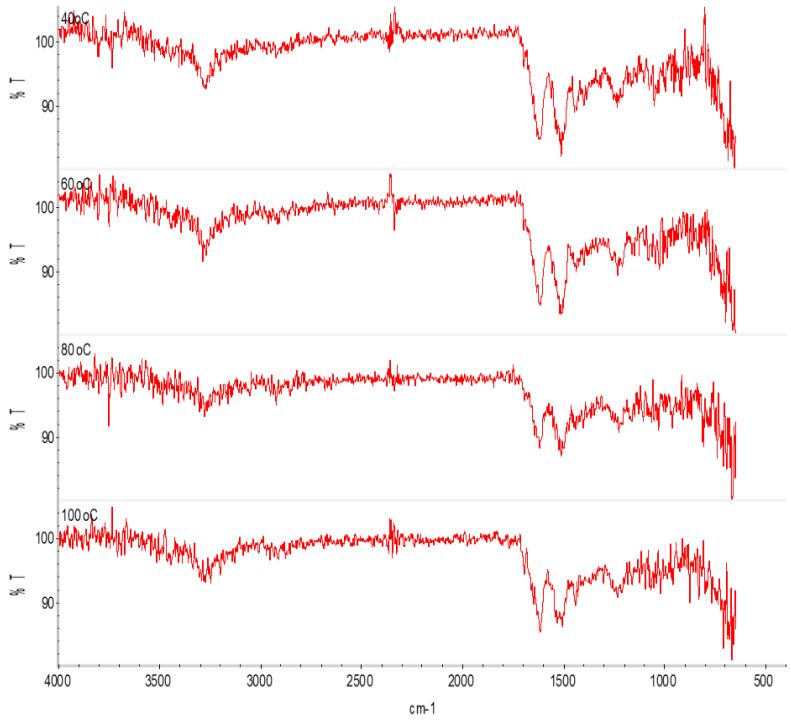

Figure 11. FTIR of dyed silk fabric with different temperatures, condition pH 5, time 45 min. and L:R. 1:40.

The amide bands in FTIR spectra with different temperatures indicate the molecular conformation of silk fabric. As Figure 11 shows, the FTIR spectra of all dyed silk fabric are degummed for various temperatures. The IR peak at1669 cm^{-1} shifted to 1640 cm^{-1}, the 1260 cm^{-1} shoulder peak disappeared, and also the samples showed similar and strong bands with increased temperature of the dye bath, the intensity of the peak of all amide groups formed (i.e., amide II, amide III, amide IV, and amide V) increase with increasing temperature from 40,60, and 80^{o}C then decrease with increasing temperature up to 100 ^{o}C. The similarity in FTIR spectra implies that assigned to the β-sheet, and α-helix conformation. Because the silk consists of light (L) chain polypeptide and a heavy (H) chain polypeptide linked together via a single disulfide bond at the C-terminus of the H-chain, forming an H–L complex [48,49].

3.2.3. X-ray diffraction (XRD) spectrometer.

Analysis XRD was used to calculate the serum crystallinity index (CI) degree. In the macromolecules of silk fabric, the formed free hydroxyl and amino groups were involved in a number of intra- and inter-molecular hydrogen bonds, which can give rise to various ordered crystalline arrangements. Three forms of silk protein conformations have been suggested [50] . Until crystallization, the glandular state is Silk I. Silk II is the spun silk state consisting of the β-sheet secondary structure, and Silk III (an air / water-assembled interfacial silk) is helical. Silk I main diffraction peaks are present at approximately 2θ = 12.2 ° and 28.2°. In comparison, Silk II is present at approximately 2θ = 18.9° and 20.7° in the present sample used of silk fabric (undyed), there are two diffraction peaks, the first peak at 2θ = 20.48 ° and the other one at 2θ = 28.39° respectively.

The first group, as shown in Figure 12, presents XRD spectra of dyed and undyed silk materials with various pH values (2, 3, 4, 5, 6, and 9). An unremarkable change in the diffraction peak position was determined from the XRD spectrum of silk fabrics after being dyed with Artemisia herb-alba (as a natural dye). We found that the best spectrum was at pH 5 for samples. As shown in Figure 13, the second group shows XRD spectra with different times of dyed and undyed silk fabrics by comparing the amplitude for all peaks were also increased by dyeing process time (15, 30,45,60, and 90 minutes). It is obvious that the spectrum has a maximum of 45 minutes, the Third group as shown in Figure 14, which shows XRD spectra with different temperatures of undyed and dyed silk fabrics. The amplitude of the peaks was increased with increasing temperature (40, 60, and 80^{o}C) compared to the undyed peaks and the large diffraction peaks. It is obvious that the spectrum has a maximum of 80^{o}C.

Glycine, alanine, and serine are the product of silk fabric (undyed). The crystalline regions of silk fabric are produced by these three basic amino acids, while the amino acids with polar side chains form the amorphous regions. The silk fabric is crystalline in part and amorphous in part. The presence of sharp reflections and diffuse dispersion observed from the XRD of pure silk (undyed), as shown in Table 4, is typical of crystalline and amorphous phases and is a linear polypeptide [51,52]. Compared with the undyed peaks and the diffraction peaks for 2θ between 20°, 25°, and 28°, the amplitude of the peaks was also increased by dyeing. It is apparent that there are several peaks in the spectrum, usually, with the crystalline structure of silk, I and silk II at about 2θ = 20 and 25.2° and some new peaks are shown at 2θ = 28°, meaning that the density of hydrogen bond and peptide bond with *Artemisia herba-alba* (as a natural dye) increased with different conditions as shown in (Table 4)the most diffraction peak was 2θ = 28°, corresponding to the silk fabric used as (002) crystallographic plane family. And also, the d-spacing (in A°) of the peaks was shown in (Table 4) the result obtained was an

arrangement with the previously reported [53] diffraction spectrum of dyed silk fabric with, which implies that the hydrogen bond density of the silk structure and partially new bonds formed with that natural dye used.

The silk fabric has various compositions of amino acids, which can contribute to different types of crystallite and molecular arrangements. Regenerated silk's crystallinity or crystallite size increases and then decreases until reaching the optimum dyeing process state, clearly in Table 4 for different conditions during the dyeing process from pH value, time, and temperature shift.

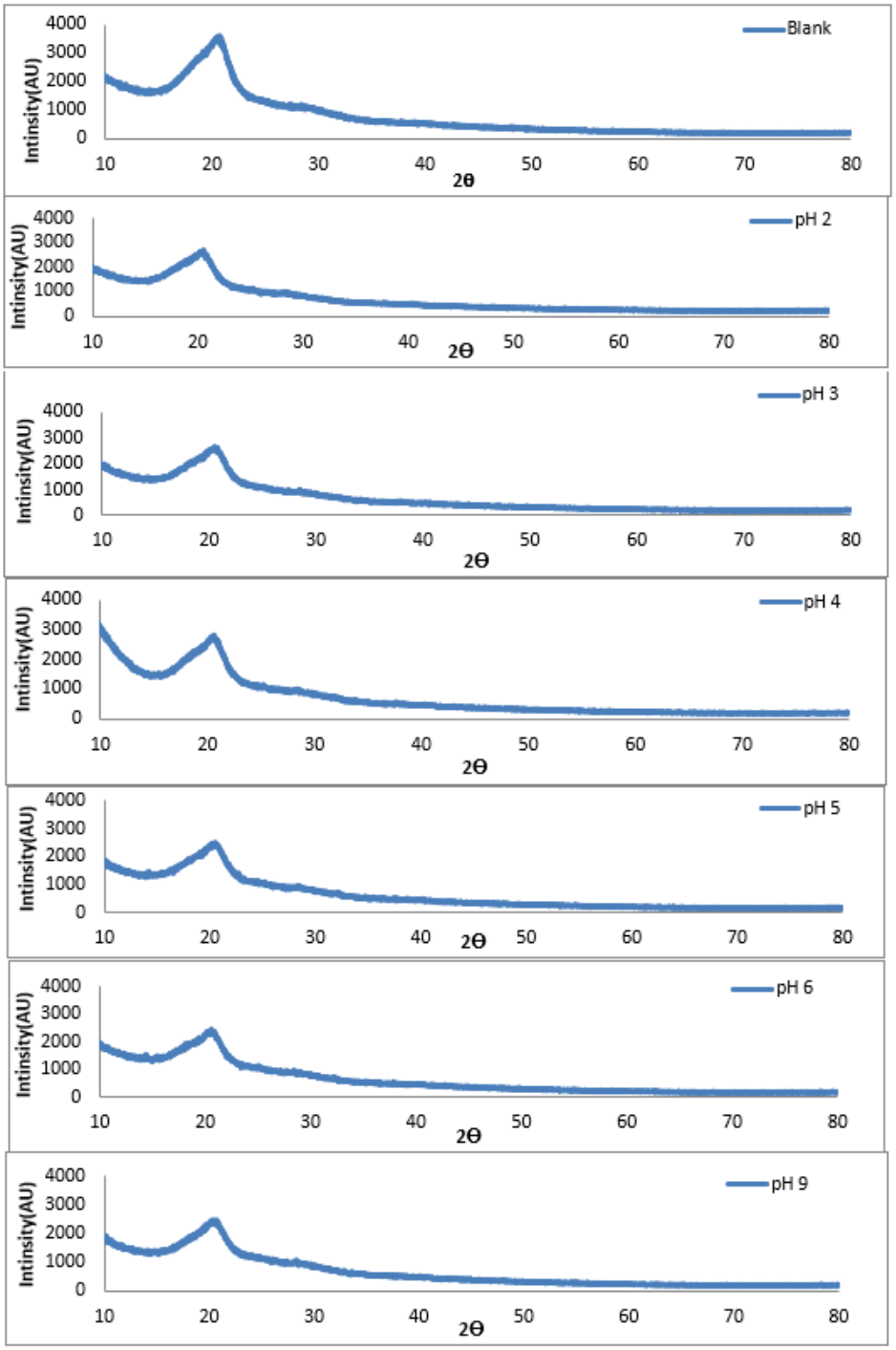

Figure 12. Variation in X-ray diffraction patterns of undyed and dyed Silk fabrics with *Artemisia herba-alba*(as natural dye) at different pH value, at temperature 80°C, time 45 min. and Lquqr ratio 1:40.

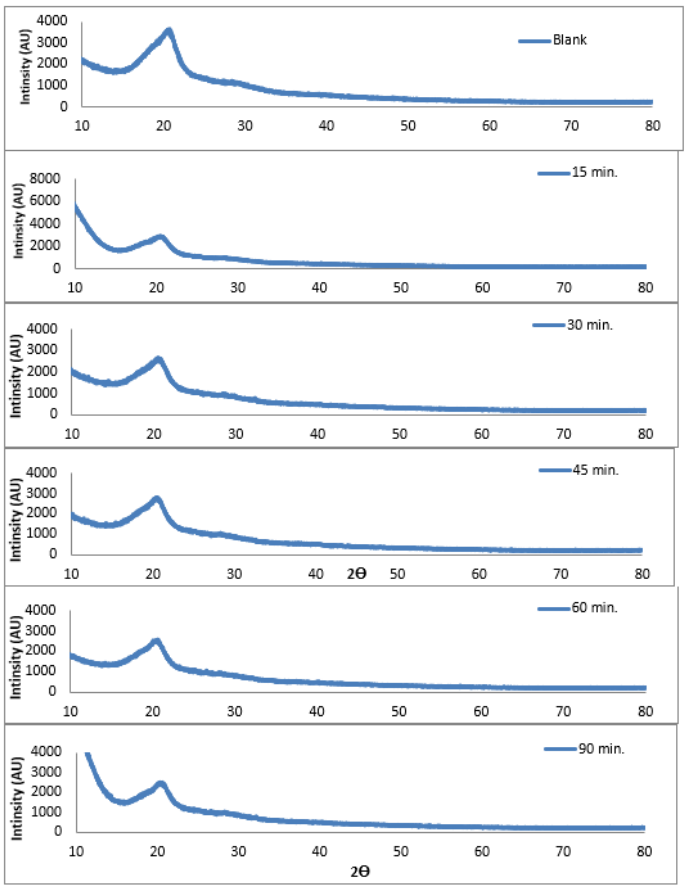

Figure 13. Variation in X-ray diffraction patterns of undyed and dyed Silk fabrics with *Artemisia herba-alba*(as natural dye) at different times, at temperature 80oC, pH 5. and L: R 1:40.

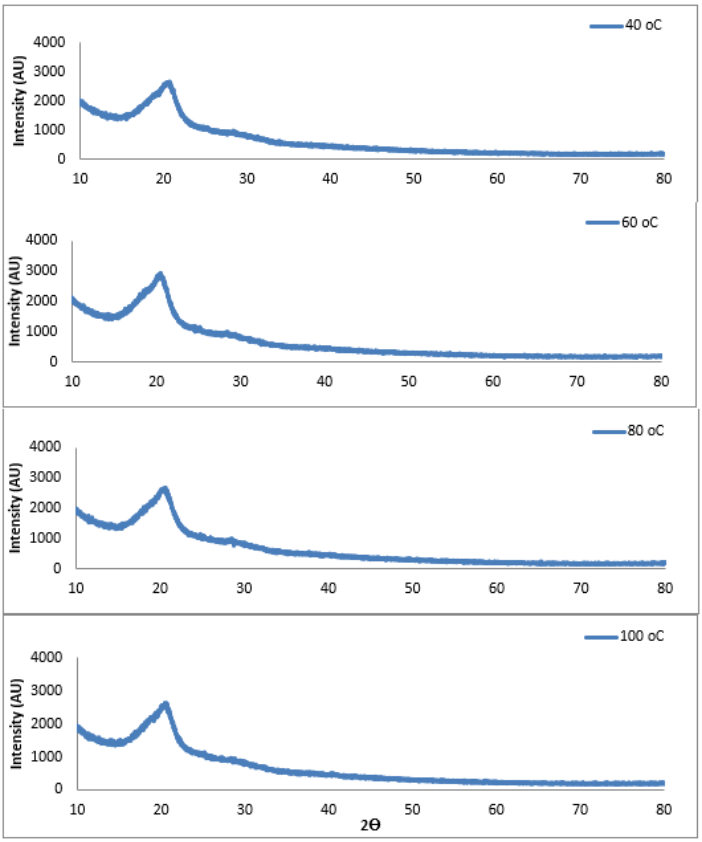

Figure 14. Variation in X-ray diffraction patterns of undyed and dyed Silk fabrics with *Artemisia herba-alba*(as natural dye) at a different temperature, at pH 5, time 45 min. and Lquqr ratio 1:40.

Table 4. XRD crystallinity index and crystallite size for all undyed and dyed silk fabrics with *Artemisia herba-alba* (as natural dye) with different conditions at L:R. 1:40.

	Silk samples	2θ (deg.)	index height (cts)	FWHM (deg.)	Crystallite size (nm)
	Blank	28.387	102.67	0.1535	3.1441
pH value	2	28.389	46.37	0.1819	3.1429
	3	28.396	54.90	0.2154	3.1441
	4	28.398	58.04	0.3070	3.1447
	5	28.410	95.45	0.6140	3.1527
	6	28.358	82.76	0.1535	3.1473
	9	28.320	81.02	0.1307	3.1414
Time	15 min.	28.373	62.73	0.3070	3.1457
	30 min.	28.385	83.13	0.6307	3.1443
	45 min.	28.410	84.88	0.8614	3.1527
	60 min.	28.318	54.50	0.8187	3.1666
	90 min.	28.182	39.70	0.8187	3.1416
Temp.	40 ºC	28.322	58.66	0.3070	3.1423
	60ºC	28.389	72.11	0.3570	3.1439
	80 ºC	28.404	84.20	0.8187	3.1527

4. Conclusions

To understand the effect of dyeing with natural dye with different conditions (pH value, time, and temperature) in comparison with undyed silk fabrics on the surface properties, experimental and analytical observations of dyed silk fabrics with Artemisia herba alba (as a natural dye) have been performed. Different characterizing techniques such as TGA, ATR-FTIR, and XRD) compared to undyed silk fabrics have examined structural improvements in silk fabric dyeing. The XRD studies revealed that the index of surface crystallinity is reduced due to hydrogen bonds between silk fabric and dye, but this leads to a decrease in the crystallinity index; the findings of XRD and ATR-FTIR are also confirmed. As a consequence of the roughness. This is considered to be an efficient outcome because specific surface area increases due to the roughness property and contributes to more silk fabric dyed, showing that the characteristic value in the continuum, i.e., transmittance increases after dyeing, and it is seen to be maximum for pH 5, 45 minutes and 80ºC dyeing conditions. And also, that is are in agreement with the obtained thermal data and might exhibit higher thermal stability (TGA) for samples used; it is suggested to dye silk fabrics with natural dye as an environmentally friendly technique to dye silk fabric.

Funding

This research received no external funding.

Acknowledgments

This research has no acknowledgment.

Conflicts of Interest

The authors declare no conflict of interest.

References

1. Bertella, A.; Benlahcen, K.; Abouamama, S.; Pinto, D.C.G.A.; Maamar, K.; Kihal, M.; Silva, A.M.S. *Artemisia herba-alba* Asso. essential oil antibacterial activity and acute toxicity. *Industrial Crops and Products* **2018**, *116*, 137-143, https://doi.org/10.1016/j.indcrop.2018.02.064.

2. Esmail, A.; Mohamed, A.; El-Sayed, M.; Hegazy, M.E.; Helaly, S.; Salaheldin, N. Chemical constituents and biological activities of *Artemisia herba-alba*. *Rec. Nat. Prod.* **2010**, *4*, 1-25, https://doi.org/10.13140/RG.2.1.2544.8806.
3. Brown F.; Driver S.R.; Briggs C.A.; Gesenius C.;. *Hebrew Lexicon entry for La'anah. The Old Testament Hebrew* Published by Lexicon. Lockman Foundation,**1998** and Retrieved 17 February **2010.**
4. Briggs, C.A.; Driver, S.R.; Brown, F. *Brown-Driver-Briggs Hebrew and English Lexicon*. Published by Snowball Publishing, **2011.**
5. Seifeddine, R.; Chibani, S.; Kabouche, A.; Kabouche, Z. Chemical composition of essential oil of aerial parts of *Artemisia herba-alba* Asso. from Oum El-Bouaghi (Algeria) and chemotaxonomic survey. *journal of material and environmental science* **2016**, *7*, 4383-4390.
6. Jaber, H.; Oubihi, A.; Ouryemchi, I.; Boulamtat, R.; Oubayoucef, A.; Bourkhiss, B.; Ouhssine, M. Chemical Composition and Antibacterial Activities of Eight Plant Essential Oils from Morocco against Escherichia coli Strains Isolated from Different Turkey Organs. *Biochemistry Research International* **2021**, *2021*, https://doi.org/10.1155/2021/6685800.
7. Ben Salha, G.; Herrera Díaz, R.; Labidi, J.; Abderrabba, M. Deterpenation of Origanum majorana L. essential oil by reduced pressure steam distillation. *Industrial Crops and Products* **2017**, *109*, 116-122, http://dx.doi.org/10.1016/j.indcrop.2017.08.016.
8. Salido, S.; Valenzuela, L.R.; Altarejos, J.; Nogueras, M.; Sánchez, A.; Cano, E. Composition and infraspecific variability of *Artemisia herba-alba* from southern Spain. *Biochemical Systematics and Ecology* **2004**, *32*, 265-277, https://doi.org/10.1016/j.bse.2003.09.002.
9. Paolini, J.; Ouariachi, E.; Bouyanzer, A.; Hammouti, B.; Desjobert, J.-M.; Costa, J.; Muselli, A. Chemical variability of *Artemisia herba-alba* Asso essential oils from East Morocco. *Chemical papers* **2010**, *64*, 550-556, https://doi.org/10.2478/s11696-010-0051-5.
10. Moufid, A.; Eddouks, M. Artemisia herba alba: a popular plant with potential medicinal properties. *Pakistan journal of biological sciences : PJBS* **2012**, *15*, 1152-1159, https://doi.org/10.3923/pjbs.2012.1152.1159.
11. Salah, S.M.; Jäger, A.K. Two flavonoids from *Artemisia herba-alba* Asso with in vitro GABAA-benzodiazepine receptor activity. *Journal of Ethnopharmacology* **2005**, *99*, 145-146, https://doi.org/10.1016/j.jep.2005.01.031.
12. Koh, L.-D.; Cheng, Y.; Teng, C.-P.; Khin, Y.-W.; Loh, X.-J.; Tee, S.-Y.; Low, M.; Ye, E.; Yu, H.-D.; Zhang, Y.-W.; Han, M.-Y. Structures, mechanical properties and applications of silk fibroin materials. *Progress in Polymer Science* **2015**, *46*, 86-110, https://doi.org/10.1016/j.progpolymsci.2015.02.001.
13. Wen, D.J.; Wang, H.; Zhu, X.S.; Sun, J.P. Conformation and crystallinity of silk fibroin. *J. Textile. Res* **2005**, *26*, 110-112.
14. Kundu, J.; Poole-Warren, L.A.; Martens, P.; Kundu, S.C. Silk fibroin/poly(vinyl alcohol) photocrosslinked hydrogels for delivery of macromolecular drugs. *Acta biomaterialia* **2012**, *8*, 1720-1729, http://dx.doi.org/10.1016/j.actbio.2012.01.004.
15. Kadakia, P.U.; Jain, E.; Hixon, K.R.; Eberlin, C.T.; Sell, S.A. Sonication induced silk fibroin cryogels for tissue engineering applications. *Materials Research Express* **2016**, *3*, https://doi.org/10.1088/2053-1591/3/5/055401.
16. Worch, J.C.; Prydderch, H.; Jimaja, S.; Bexis, P.; Becker, M.L.; Dove, A.P. Stereochemical enhancement of polymer properties. *Nature Reviews Chemistry* **2019**, *3*, 514-535, https://doi.org/10.1038/s41570-019-0117-z.
17. Wang, H.-Y.; Zhang, Y.-Q. Processing and characterisation of a novel electropolymerized silk fibroin hydrogel membrane. *Scientific Reports* **2014**, *4*, https://doi.org/10.1038/srep06182.
18. Tsukada, M.; Freddi, G.; Monti, P.; Bertoluzza, A.; Kasai, N. Structure and molecular conformation of tussah silk fibroin films: Effect of methanol. *Journal of Polymer Science Part B: Polymer Physics* **1995**, *33*, 1995-2001, https://doi.org/10.1002/polb.1995.090331402.
19. Park, S.J.; Lee, K.Y.; Ha, W.S.; Park, S.Y. Structural changes and their effect on mechanical properties of silk fibroin/chitosan blends. *Journal of Applied Polymer Science* **1999**, *74*, 2571-2575, https://doi.org/10.1002/(SICI)1097-4628(19991209)74:11<2571::AID-APP2>3.0.CO;2-A.
20. Gil, E.S.; Panilaitis, B.; Bellas, E.; Kaplan, D.L. Functionalized silk biomaterials for wound healing. *Adv Healthc Mater* **2013**, *2*, 206-217, https://doi.org/10.1002/adhm.201200192.
21. Guan, J.; Yang, C.Q.; Chen, G. Formaldehyde-free flame retardant finishing of silk using a hydroxyl-functional organophosphorus oligomer. *Polymer Degradation and Stability* **2009**, *94*, 450-455, https://doi.org/10.1016/j.polymdegradstab.2008.10.024.
22. Hardy, J.G.; Römer, L.M.; Scheibel, T.R. Polymeric materials based on silk proteins. *Polymer* **2008**, *49*, 4309-4327, https://doi.org/10.1016/j.polymer.2008.08.006.
23. Zhou, C.-Z.; Confalonieri, F.; Medina, N.; Zivanovic, Y.; Esnault, C.; Yang, T.; Jacquet, M.; Janin, J.; Duguet, M.; Perasso, R.; Li, Z.-G. Fine organization of Bombyx mori fibroin heavy chain gene. *Nucleic acids research* **2000**, *28*, 2413-2419, https://doi.org/10.1093/nar/28.12.2413.
24. Inoue, S.; Tanaka, K.; Arisaka, F.; Kimura, S.; Ohtomo, K.; Mizuno, S. Silk Fibroin of *Bombyx mori* Is Secreted, Assembling a High Molecular Mass Elementary Unit Consisting of H-chain, L-chain, and P25, with

a 6:6:1 Molar Ratio *. *Journal of Biological Chemistry* **2000**, *275*, 40517-40528, https://doi.org/10.1074/jbc.M006897200.
25. Anonymous. Fibre2Fashion.com. National gem of China – the silk industry; 2009. http://www.fibre2fashion.com/industry-article/17/1631/national-gem-of-china-the-silk-industry1.asp [accessed June **2013**].
26. Koh, L.-D.; Cheng, Y.; Teng, C.-P.; Khin, Y.-W.; Loh, X.-J.; Tee, S.-Y.; Low, M.; Ye, E.; Yu, H.-D.; Zhang, Y.-W.; Han, M.-Y. Structures, mechanical properties and applications of silk fibroin materials. *Progress in Polymer Science* **2015**, *46*, 86-110, http://dx.doi.org/10.1016/j.progpolymsci.2015.02.001.
27. Sheikh, M.R.K.; Farouqui, F.I.; Modak, P.R.; Hoque, M.A.; Yasmin, Z. Dyeing of Rajshahi silk with basic dyes: Effect of modification on dyeing properties. *The Journal of The Textile Institute* **2006**, *97*, 295-300, https://doi.org/10.1533/joti.2005.0118.
28. Ki, C.S.; Kim, J.W.; Oh, H.J.; Lee, K.H.; Park, Y.H. The effect of residual silk sericin on the structure and mechanical property of regenerated silk filament. *International Journal of Biological Macromolecules* **2007**, *41*, 346-353, https://doi.org/10.1016/j.ijbiomac.2007.05.005.
29. Kim, H.J.; Um, I.C. Effect of degumming ratio on wet spinning and post drawing performance of regenerated silk. *International Journal of Biological Macromolecules* **2014**, *67*, 387-393, http://dx.doi.org/10.1016/j.ijbiomac.2014.03.055.
30. Yun, H.; Oh, H.; Kim, M.K.; Kwak, H.W.; Lee, J.Y.; Um, I.C.; Vootla, S.K.; Lee, K.H. Extraction conditions of Antheraea mylitta sericin with high yields and minimum molecular weight degradation. *International Journal of Biological Macromolecules* **2013**, *52*, 59-65, http://dx.doi.org/10.1016/j.ijbiomac.2012.09.017.
31. Yoon, K.; Lee, H.N.; Ki, C.S.; Fang, D.; Hsiao, B.S.; Chu, B.; Um, I.C. Effects of degumming conditions on electro-spinning rate of regenerated silk. *International Journal of Biological Macromolecules* **2013**, *61*, 50-57, https://doi.org/10.1016/j.ijbiomac.2013.06.039.
32. Speakman, J.B. The Structure of the Wool Fibre; its Relation to the Dyeing and Finishing Processes of the Wool Textile Trade. *Journal of the Society of Dyers and Colourists* **1933**, *49*, 180-194, https://doi.org/10.1111/J.1478-4408.1933.TB01757.X.
33. Jonson J. *The Theory of Coloration of textiles*. Society of dyers and Colorists,Bradford. **1990.**
34. Marin-Bustamante, M.Q.; Chanona-Pérez, J.J.; Güemes-Vera, N.; Cásarez-Santiago, R.; PereaFlores, M.J.; Arzate-Vázquez, I.; Calderón-Domínguez, G. Production and characterization of cellulose nanoparticles from nopal waste by means of high impact milling. *Procedia Engineering* **2017**, *200*, 428-433, https://doi.org/10.1016/j.proeng.2017.07.060.
35. Nam, S.; French, A.D.; Condon, B.D.; Concha, M. Segal crystallinity index revisited by the simulation of X-ray diffraction patterns of cotton cellulose Iβ and cellulose II. *Carbohydrate Polymers* **2016**, *135*, 1-9, https://doi.org/10.1016/j.carbpol.2015.08.035.
36. Ray, S.S.; Salehiyan, R. Chapter 5 - Processing techniques and structural and morphological characterization. In: *Nanostructured Immiscible Polymer Blends*. Ray, S.S.; Salehiyan, R. Eds.; Elsevier: **2020**; pp. 81-98, http://dx.doi.org/10.1016/B978-0-12-816707-6.00005-5.
37. Sudha, S.; Thilagavathi, G. Analysis of electrical, thermal and compressive properties of alkali-treated jute fabric reinforced composites. *Journal of Industrial Textiles* **2017**, *47*, 1407-1423, https://doi.org/10.1177/1528083717695840.
38. . Nakamura, S.; Magoshi, J.; Magoshi, Y. Thermal Properties of Silk Proteins in Silkworms. In *Silk Polymers*; ACS Symposium Series; American Chemical Society: Volume 544, **1993;** pp. 211-221, https://doi.org/10.1021/bk-1994-0544.ch019.
39. Zhao, L.; Luo, J.; Wang, H.; Song, G.; Tang, G. Self-assembly fabrication of microencapsulated n-octadecane with natural silk fibroin shell for thermal-regulating textiles. *Applied Thermal Engineering* **2016**, *99*, 495-501, https://doi.org/10.1016/j.applthermaleng.2015.12.111.
40. Shaabani, A.; Hezarkhani, Z.; Badali, E. Natural silk supported manganese dioxide nanostructures: Synthesis and catalytic activity in aerobic oxidation and one-pot tandem oxidative synthesis of organic compounds. *Polyhedron* **2016**, *107*, 176-182, http://dx.doi.org/10.1016/j.poly.2016.01.019.
41. Shigeo, N.; Jun, M.; Yoshiko, M. Thermal Properties of Silk Proteins in Silkworms. In: *Silk Polymers.* **2014**; pp. 211–221, https://doi.org/10.1021/bk-1994-0544.ch019.
42. Wahab, L.A.; El-Zaher, N.A. Effect of irradiation on thermal properties of poly (vinyl chloride). *Egyptian Journal of solids* **1996**, *19*, 271-279.
43. Rusa, C.C.; Bridges, C.; Ha, S.-W.; Tonelli, A.E. Conformational Changes Induced in Bombyx mori Silk Fibroin by Cyclodextrin Inclusion Complexation. *Macromolecules* **2005**, *38*, 5640-5646, https://doi.org/10.1021/ma050340a.
44. Byler, D.M.; Susi, H. Examination of the secondary structure of proteins by deconvolved FTIR spectra. *Biopolymers: Original Research on Biomolecules* **1986**, *25*, 469-487, https://doi.org/10.1002/bip.360250307.
45. Krimm, S.; Bandekar, J. Vibrational Spectroscopy and Conformation of Peptides, Polypeptides, and Proteins. In: *Advances in Protein Chemistry*. Anfinsen, C.B.; Edsall, J.T.; Richards, F.M. Eds.; Academic Press: Volume 38, **1986**; pp. 181-364, http://dx.doi.org/10.1016/S0065-3233(08)60528-8.

46. Dousseau, F.; Therrien, M.; Pézolet, M. On the Spectral Subtraction of Water from the FT-IR Spectra of Aqueous Solutions of Proteins. *Applied Spectroscopy* **1989**, *43*, 538-542, https://doi.org/10.1366%2F0003702894202814.
47. Li, M.; Tao, W.; Kuga, S.; Nishiyama, Y. Controlling molecular conformation of regenerated wild silk fibroin by aqueous ethanol treatment. *Polymers for Advanced Technologies* **2003**, *14*, 694-698, https://doi.org/10.1002/pat.409.
48. Yamaguchi, K.; Kikuchi, Y.; Takagi, T.; Kikuchi, A.; Oyama, F.; Shimura, K.; Mizuno, S. Primary structure of the silk fibroin light chain determined by cDNA sequencing and peptide analysis. *Journal of Molecular Biology* **1989**, *210*, 127-139, https://doi.org/10.1016/0022-2836(89)90295-7.
49. Zhou, C.-Z.; Confalonieri, F.; Medina, N.; Zivanovic, Y.; Esnault, C.; Yang, T.; Jacquet, M.; Janin, J.; Duguet, M.; Perasso, R.; Li, Z.-G. Fine organization of Bombyx mori fibroin heavy chain gene. *Nucleic acids research* **2000**, *28*, 2413-2419, https://doi.org/10.1093/nar/28.12.2413.
50. Lamoolphak, W.; De-Eknamkul, W.; Shotipruk, A. Hydrothermal production and characterization of protein and amino acids from silk waste. *Bioresource Technology* **2008**, *99*, 7678-7685, https://doi.org/10.1016/j.biortech.2008.01.072.
51. Puttanna, P.; Rudrappa, S. Crystal Structure of Locally Available Tassar Fibers Based on [Ala-Gly] *International Scholarly Research Notices* **2011**, *2011*, https://doi.org/10.5402/2011/857432.
52. Patel, J.P.; Parsania, P.H. 3 - Characterization, testing, and reinforcing materials of biodegradable composites. In: *Biodegradable and Biocompatible Polymer Composites*. Shimpi, N.G. Ed.; Woodhead Publishing: **2018**; pp. 55-79, https://doi.org/10.1016/B978-0-08-100970-3.00003-1.
53. Wu, J.-H.; Wang, Z.; Xu, S.-Y. Preparation and characterization of sericin powder extracted from silk industry wastewater. *Food Chemistry* **2007**, *103*, 1255-1262, https://doi.org/10.1016/j.foodchem.2006.10.042.